FEL stochastic spectroscopy showcasing silicon bond softening dynamics

Supplemental Material

Dario De Angelis[1]* Emiliano Principi[1], Filippo Bencivenga[1], Daniele Fausti[1,2,3], Laura Foglia[1], Yishay Klein[4], Michele Manfredda[1], Riccardo Mincigrucci[1], Angela Montanaro[1,2], Emanuele Pedersoli[1], Jacopo Stefano Pelli Cresi[1], Giovanni Perosa[1], Kevin C. Prince[1], Elia Razzoli[5], Sharon Shwartz[4], Alberto Simoncig[1], Simone Spampinati[1], Cristian Svetina[5], Jakub Szlachetko[6], Alok Tripathi[4], Ivan A. Vartanyants[7], Marco Zangrando[1,8], and Flavio Capotondi[1]

[1]*Elettra-Sincrotrone Trieste, Strada Statale 14-km 163.5, Basovizza, 34149, Trieste, Italy*
[2]*Department of Physics, Università degli Studi di Trieste, 34127, Trieste, Italy*
[3]*Lehrstuhl für Festkörperphysik, Friedrich-Alexander-Universität Erlangen-Nürnberg, Erlangen 91058, Germany;*
[4]*Physics Department and Institute of Nanotechnology and advanced Materials, Bar Ilan University, Ramat Gan, 52900, Israel*
[5]*Paul Scherrer Institut, CH-5232 Villigen, Switzerland*
[6]*SOLARIS National Synchrotron Radiation Centre, Jagiellonian University, Czerwone Maki 98, 30-392 Krakow, Poland*
[7]*Deutsches Elektronen-Synchrotron DESY, Notkestr. 85, 22607 Hamburg, Germany*
[8]*Istituto Officina dei Materiali, CNR, Strada Statale 14-km 163.5, Basovizza, 34149, Trieste, Italy*

* deangelis@iom.cnr.it

DATA ANALYSIS

To retrieve the XAS and XES spectra of c-Si, we analyzed the spectra acquired upstream and downstream of the sample by applying the correlation spectroscopy method described by Kayser [1]. In this framework, the incident and transmitted light spectra measured by the two spectrometers (see Fig. S1) are accumulated into two bidimensional tensors, A_{ij} and B_{ik}, respectively, in which the i-th row is the photon energy spectrum of a single FEL shot. In this way, the sample transfer matrix, x_{jk}, that maps the incoming spectra into the outgoing ones can be calculated by solving the linear equation:

$$Ax = B\,. \qquad (1)$$

The off-diagonal terms in x can be directly interpreted as the Inelastic X-ray Scattering (IXS) map, while the diagonal terms represent the absorption (elastic) response of the sample at the energy determined by the two spectrometers. FEL pulses with different spectral content can be regarded as linearly independent vectors in the photon energy space. Assuming that the stochastic pulses are all linearly independent, to solve the linear system in (1), it is necessary to accumulate a number i of FEL pulses equal to the number of spectral bins. It has been demonstrated that the large variability in the photon energy distribution, provided by the SASE-like FEL emission, is the key feature that makes this correlation spectroscopic methods extremely efficient [1–3]. The stochastic spectral variability of the SASE-like mode indeed ensures coverage of the entire energy space.

Considering N samples per spectrum, we have an N-dimensional vector basis in our energy space, we thus need the same number of linearly independent FEL pulses to completely solve the linear system of equations relating the input and output spectra. Nonetheless, in our experience, we observed that we need at least 50 to 100 times more pulses than N, which means from 50,000 to 100,000 pulses (corresponding to 15–30 min of acquisition) for N = 1000. That is the experimental requirement to have a statistically good signal-to-noise ratio in the retrieved elements of x; this can be attributed to the finite dynamic range and signal-to-noise ratio of the detector. With a number of vectors larger than the dimension of the basis, the linear problem is over-defined, therefore the dataset has to be divided into subsets and the linear problem solved separately for each one; as a final step we averaged the obtained response matrices. To solve the linear

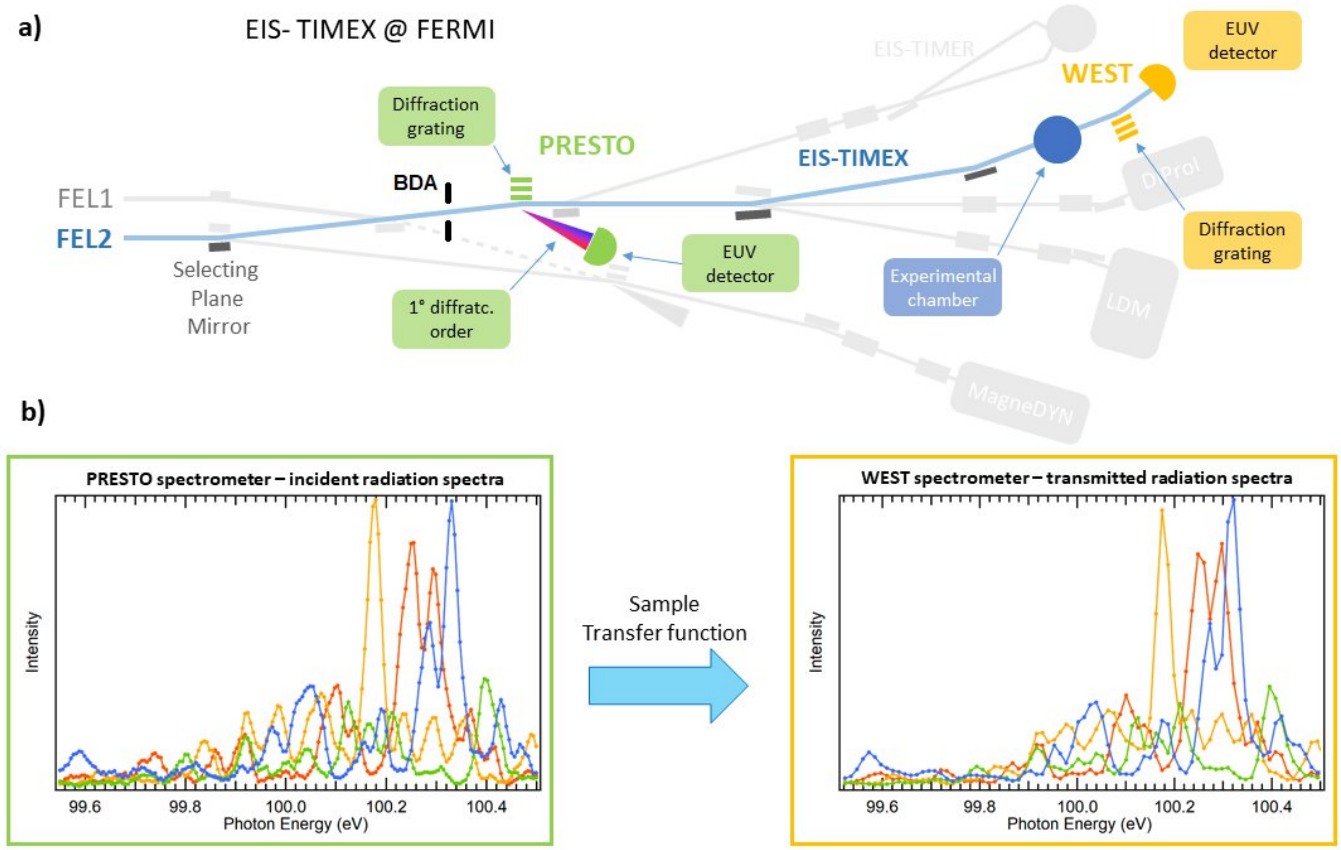

FIG. S1. (a) Scheme of the TIMEX beamline. The light blue path represents the selected beam transport. (b) Examples of 4 consecutive SASE-like pulse spectra produced by FERMI around the photon energy corresponding to the Si $L_{2,3}$-edge. The measured spectra are recorded by the two spectrometers, labelled in the figure as "PRESTO" and "WEST", placed upstream and downstream the sample, respectively.

problem, we used the Singular Value Decomposition (SVD) approach, expressing A as:

$$A = U\Sigma V^{\mathrm{T}} = \sum_{i=1}^{n} u_i \sigma_i v_i^{\mathrm{T}} \ , \qquad (2)$$

where U and V are unitary transformation matrices, (V^{T} is the transpose of V), Σ is the diagonal SVD matrix and σ_i are the corresponding eigenvalues. According to this formulation, the solution of the problem can be expressed as:

$$x = \sum_{i=1}^{n} \frac{(u_i^{\mathrm{T}} B) v_i}{\sigma_i} \ , \qquad (3)$$

from which we can observe that the smaller singular values result in the amplification of experimental errors in A and B. We employed the Tikhonov regularization method to overcome this issue [4, 5]. This regularization can be formulated as a minimization procedure of the form:

$$\min_x \left\{ \|Ax - B\|_2^2 + \lambda^2 \|\mathrm{L}x\|_2^2 \right\} \qquad (4)$$

where L is the identity matrix and λ is a real parameter. In this way, each singular value from the decomposition is weighted by a filter function f, that stabilizes the solution, i.e.:

$$x_\lambda = \sum_{i=1}^{n} f_i \frac{\left(u_i^{\mathrm{T}} B\right) v_i}{\sigma_i} \ , \qquad f_i = \frac{\sigma_i^2}{\sigma_i^2 + \lambda} \ . \qquad (5)$$

As recently described by Fuller and coworkers' noise in the diagnostic of the SASE spectrum has strong impact on the regression of sample response matrix, especially in the pre- and post-edge region of an absorption spectra [6]. For example, spatio-spectral variation within the beam profile, potentially filtered by the photon-beam transport, can alter the correlation between PRESTO and WEST spectrometers even without sample, creating artifact in the reconstruction of the transfer matrix x. For this reason, the correlation between the two spectrometers has been optimized using beam defined apertures (BDA) placed upstream PRESTO spectrometer. A clear improvement in the relative correspondence between the recorded spectra is observed when the BDA clearance aperture is reduced along the horizontal plant from 3.0 mm to 1.5 mm, while the vertical dimension was keep fixed to 3.0 mm. A representative example of the two above reported conditions for BDA aperture is shown in the Figures S2 (a) and (b) respectively. The experimental data show a worst correspondence between the two recorded spectra at PRESTO and WEST when the BDA was set at a clearance aperture of 3.0 mm with respect to smaller dimension of filtering slits. The worst correlation between the PRESTO and WEST spectrum under the condition of large BDA clearance manifests itself either with larger broadening of the single SASE spikes for WEST spectrometer and either a larger intensity fluctuation between the two spectra. The broadening of spectral lines of WEST spectrometer for larger BDA clearance hole is also evident in the comparison of the width of the $g^{(2)}(\omega_1,\omega_2)$ map (see next section for the definition of $g^{(2)}$ function) evaluated along the direction $\omega_2 = -\omega_1$. The line shape for 3.0 mm width BDA of the $g^{(2)}$ function calculated with WEST spectra has a larger width than $g^{(2)}$ function reconstructed with the same data collected with the PADRES spectrometer (Fig. S2 (c)), while for 1.5 mm BDA setting the calculated $g^{(2)}$ functions of the two spectrometers are nearly indistinguishable. This suggest that in former case unfiltered spatio-spectral variation within the beam profile influence the diagnostic of SASE spectrum, while in the latter case the two spectrometers collect the same information. Indeed, in the first case the projection of the 3.0 mm beam dimension, defined by the BDA, on the mirror of PRESTO spectrometer, is slightly larger than the length of the area machined with grating [7], suggesting that

the un-probed part of the FEL beam has a different spectral content of the internal part.

Having proved the good correspondence of the spectra recorded on the two on-line spectrometers used in the experiment, an estimation of the energy resolution provided by our approach can be done by carrying out measurements without a sample, i.e. by correlating shot to shot the spectral features recorded by the two spectrometers (see Fig. S3(a)). In this case we expect to obtain an IXS map consisting of a transformation matrix proportional to the identity matrix, i.e. without off-diagonal terms, broadened by the finite energy resolution of the two spectrometers. Figure S3(b) displays the transverse profile of the diagonal line shown in Fig. S3(a), along with a line-shape fit with a Gaussian function, which indicates a variance (σ) of about 15 meV. This value is entirely consistent with the squared sum of the energy resolution of the two spectrometers (i.e. ≈10 meV at 100 eV for both), thus indicating that the employed inversion method does not introduce appreciable contributions to the energy resolution of more than a few meV.

FEL SOURCE CHARACTERIZATION

As recently demonstrated [8], the FERMI FEL in seeded mode fulfills the definition of a laser source proposed by Glauber [9], i.e. the emission is coherent at all orders of intensity correlation functions and is characterized by the emission of a few (in the ideal case, one) longitudinal modes. However, as described in the previous section, since the sample response is retrieved by solving a linear matrix problem, the spectral content of the input spectrum should uniformly samples the energy range of interest. In other words,

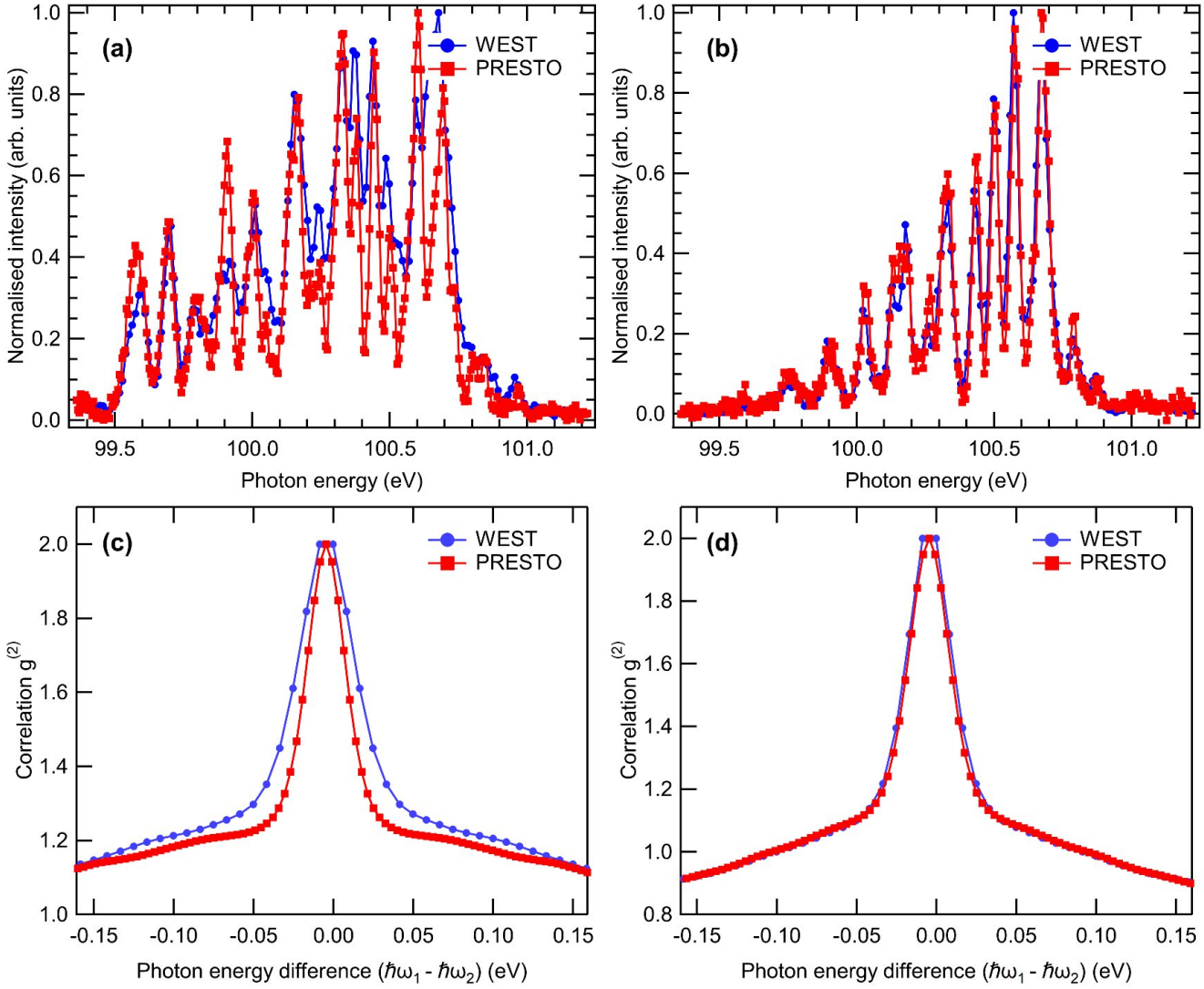

FIG. S2. (a) WEST and PRESTO spectra of the same FEL pulse, acquired with horizontal BDA set at 3 mm. (b) WEST and PRESTO spectra of the same FEL pulse, acquired with horizontal BDA set at 1.5 mm. (c) $g^{(2)}$ correlation function calculated on spectra acquired with horizontal BDA at 3 mm. (d) $g^{(2)}$ correlation function calculated on spectra acquired with horizontal BDA at 1.5 mm.

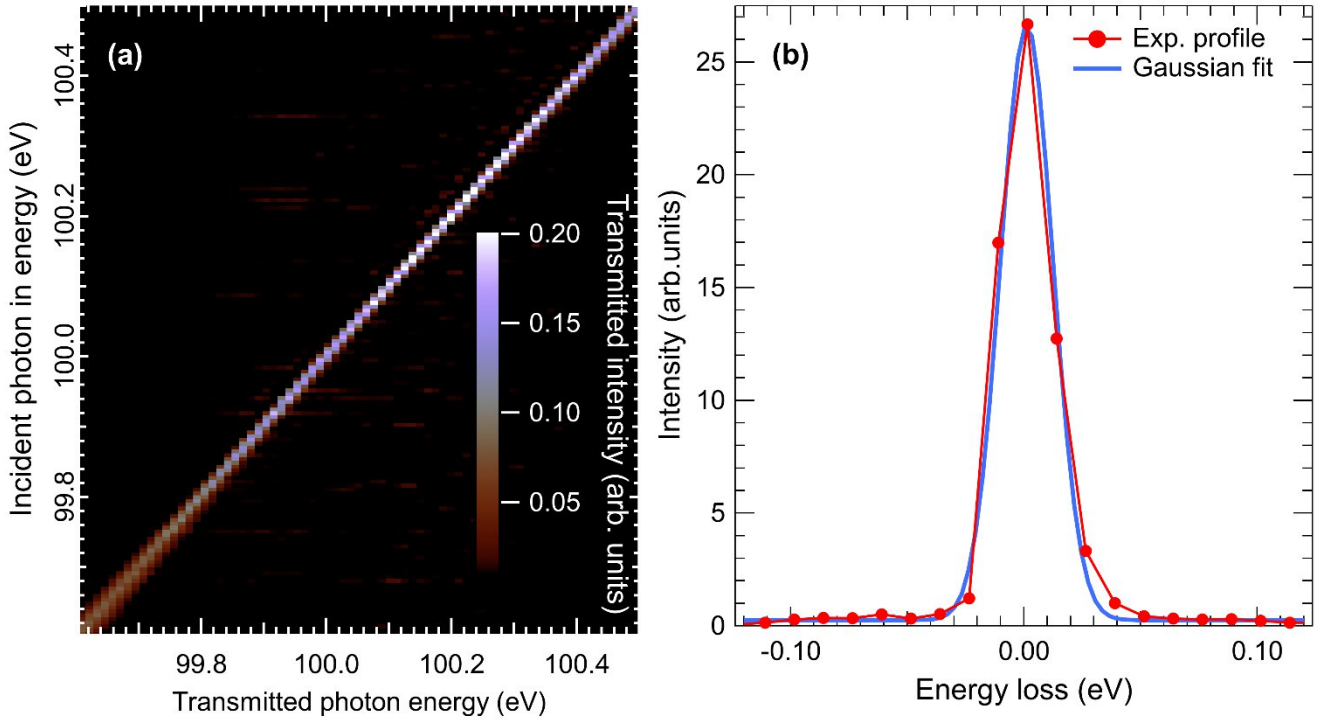

FIG. S3. (a) Correlation plot obtained without any sample in the beam path. (b) Transverse profile of the elastic line (diagonal line in panel (a)), integrated between 99.8 and 100.4 eV. Dotted line corresponds to the experimental points, solid line is the Gaussian fit.

the correlation between the different spikes forming the spectrum should be minimized, such that a direct relation between the individual spikes produced by the source and the sample response can be inferred. As shown by Fuller et al. [6], the condition of a low mutual coherence in source emission is an essential prerequisite to have superior performance in terms of acquisition time for stochastic recovered sample map compared to monochromatic energy raster scan. For this reason, here we characterize the emission of FERMI in SASE-like mode, which can be regarded as a thermal and stochastic source.

The statistical properties of the SASE-like emission as a function of the relevant parameter of the FEL source, i.e. the peak current (I_{peak}) in the linear accelerating section, were analyzed using the second-order spectral correlation function, defined as [10–14]:

$$g^{(2)}(\omega_1,\omega_2) = \frac{\langle S(\omega_1) S(\omega_2)\rangle}{\langle S(\omega_1)\rangle \langle S(\omega_2)\rangle} , \qquad (6)$$

where $S(\omega_i)$ is the spectral intensity at frequency ω_i (i=1,2) and $\langle\ \ \rangle$ denotes the average of a large ensemble of shots, equal to the number of shots used for the measurement. In addition, we considered the intensity distribution statistics to determine the number of emitted longitudinal modes, by using the Gamma probability distribution function [15]:

$$P\left(\frac{I}{\langle I\rangle}\right) = \frac{M^M}{\Gamma(M)}\left(\frac{I}{\langle I\rangle}\right)^{M-1} exp\left(-M\frac{I}{\langle I\rangle}\right) , \qquad (7)$$

where I is the total intensity measured by the spectrometer in a single shot, $\langle I\rangle$ is the intensity averaged over many pulses, and M is the number of radiated longitudinal modes.

According to the Gaussian-Schell model for partially coherent beams [16, 17], the cross-spectral density function in the frequency domain can be written as [18]:

$$W(\omega_1,\omega_2) = exp\left[-\frac{\omega_1^2+\omega_2^2}{4\Omega^2} - \frac{(\omega_2-\omega_1)^2}{2\Omega_c^2}\right] \qquad (8)$$

where Ω is the root mean square (rms) spectral bandwidth of radiation centered at a frequency ω_0, and Ω_c is the spectral coherence that can be evaluated for a thermal source by fitting the width of the antidiagonal profile of $g^{(2)}(\omega_1,\omega_2 = -\omega_1)$.

Under the assumption of a thermal source of radiation, the parameters Ω and Ω_c can be linked to the rms pulse duration τ and coherence time τ_c (rms) as [16–18]:

$$\Omega^2 = \frac{1}{\tau_c^2} + \frac{1}{4\tau^2} \; and \;\; \Omega_c = \frac{\tau_c}{\tau}\Omega \quad . \qquad (9)$$

In Fig. S4(a)–S4(c) we report a few single shot spectra collected by the PRESTO spectrometer at different values of I_{peak}, the corresponding $g^{(2)}(\omega_1,\omega_2)$ map

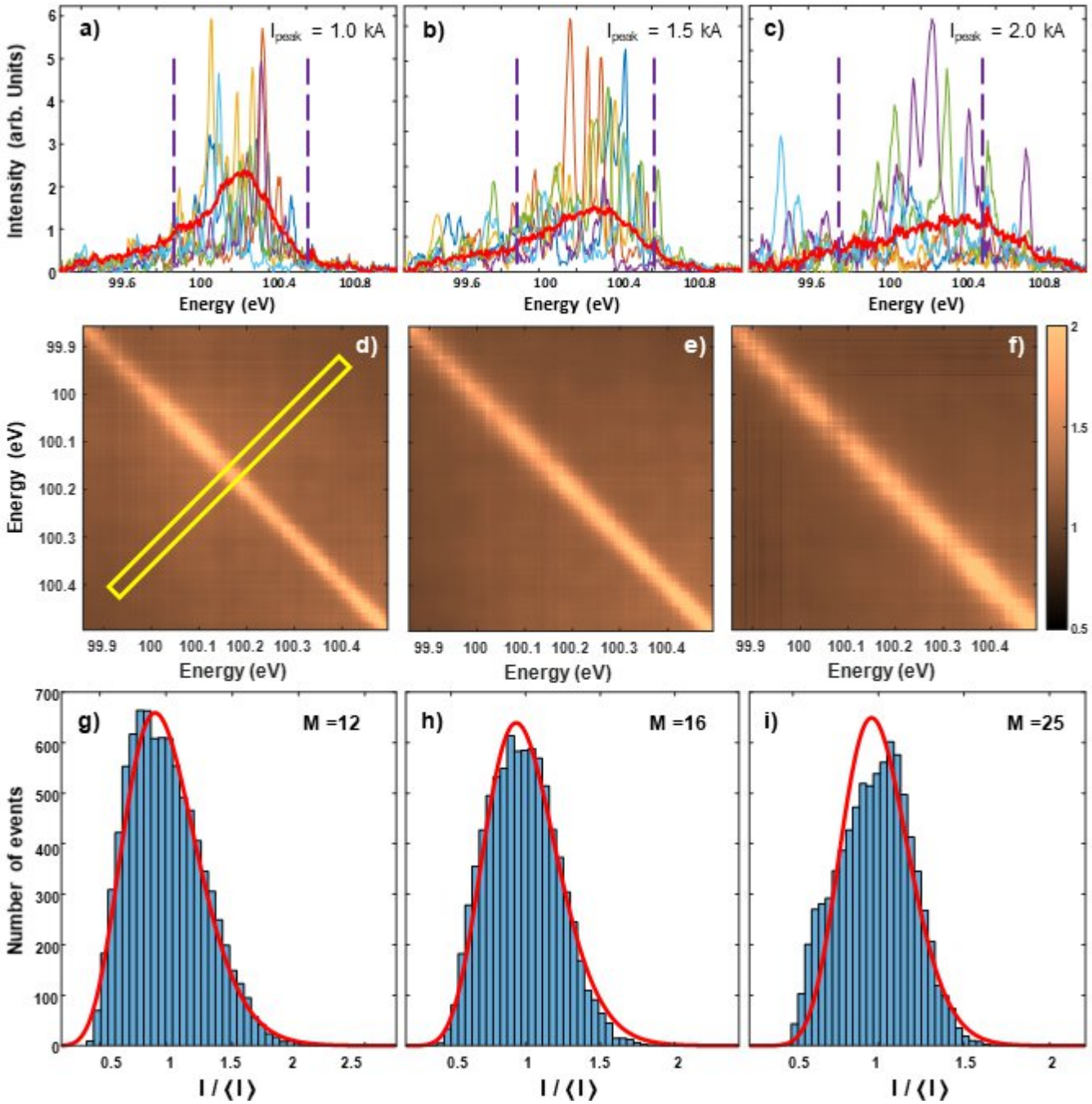

FIG. S4. (a)–(c) Sequence of 5 successive independent shots recorded by the PRESTO spectrometer for different values of I_{peak}: 1.0 kA, 1.5 kA and 2.0 kA, as indicated in the individual panels; the red curve is the average SASE-like spectrum in the three conditions. (d)–(f) Corresponding $g^{(2)}(\omega_1,\omega_2)$ spectral correlation function in the wavelength range indicated by the dashed magenta vertical lines in panels (a)–(c); in panel (d), the yellow box indicates the antidiagonal profile used for evaluating the spectral coherence in the three cases. (g)–(i) Histogram of the intensity emitted by the source in the three considered conditions. Red curves represent the best fit with Eq. (7), the corresponding value of M is indicated in the individual panels.

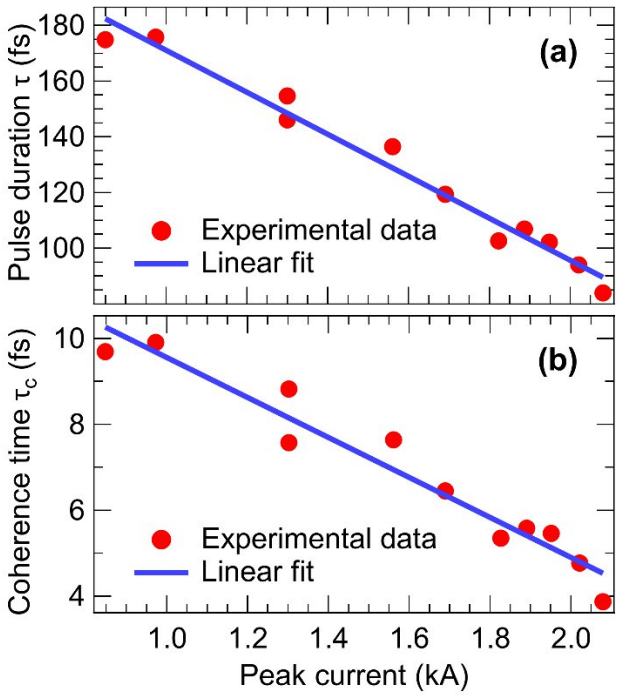

FIG. S5: (a) Dependence of the pulse duration τ on the peak current I_{peak}, as retrieved from the statistical properties of the source (Eq. (8) and (9)). (b) Same as (a) for coherence time τ_c. A linear fit is displayed on top of both graphs.

(Figures S4(d)–S4(f)), and the normalize intensity distributions (Figures S4(g)–S4(i)). The effect of increasing I_{peak} is twofold: i) on the one hand it produces a larger width of the single individual spikes in the SASE-like spectra, as evident in the $g^{(2)}(\omega_1,\omega_2)$ correlation map, where a broadening of the diagonal cross-correlation peak is observed (see Fig. S4(d)–S4(f)), while no additional features are visible outside the diagonal, compatibly with the assumption that the FEL source can be considered a stochastic thermal source; ii) On the other hand, the value of M increases, as evident from the fitting of the normalized intensity distribution, from 12 to 25 on increasing I_{peak} from 1.0 kA to 2.0 kA; see Fig. S4(g)–S4(i). This is consistent with the estimated trend of rms pulse durations and coherence time, τ and τ_c, as determined from Eq. (9); see Fig. S5(a) and S5(b). The reported data show that both τ and τ_c decrease almost linearly by increasing I_{peak}. In this way it was also possible to improve the experimental temporal resolution and obtain a more uniform distribution of the spikes in the radiation spectrum. In the experiment reported in the main article, we operate with a source setting producing a SASE pulse having an estimated duration to about 120±10 fs in rms, corresponding to 280±30 fs in full width half maximum.

REFERENCES

[1] Y. Kayser, C. Milne, P. Juranić, L. Sala, J. Czapla-Masztafiak, R. Follath, M. Kavčič, G. Knopp, J. Rehanek, W. Błachucki, M. G. Delcey, M. Lundberg, K. Tyrała, D. Zhu, R. Alonso-Mori, R. Abela, J. Sá, and J. Szlachetko, "Core-level nonlinear spectroscopy triggered by stochastic X-ray pulses", *Nat. Commun.* **10**, 1 (2019).

[2] G. Sparapassi, S. M. Cavaletto, J. Tollerud, A. Montanaro, F. Glerean, A. Marciniak, F. Giusti, S. Mukamel, and D. Fausti" Transient measurement of phononic states with covariance-based stochastic spectroscopy", *Light Sci Appl.* **11**, 1 (2022).

[3] T. J. Lane, and D. Ratner, "What are the advantages of ghost imaging? Multiplexing for x-ray and electron imaging", *Opt. Express* **28,** 5898 (2020).

[4] P. C. Hansen, and D. P. O'Leary, "The Use of the L-Curve in the Regularization of Discrete Ill-Posed Problems", *SIAM J. Sci. Comput*. **14**, 1487, (1993).

[5] D. Calvetti, S. Morigi, L. Reichel, and F. Sgallari, "Tikhonov regularization and the L-curve for large discrete ill-posed problems", *J. Comput. Appl. Math.* **123**, 423 (2000).

[6] F. D. Fuller, A. Loukianov, T. Takanashi, D. You, Y. Li, K. Ueda, T. Fransson, M. Yabashi, T. Katayama, T.-C. Weng, R. Alonso-Mori, U. Bergmann, J. Kern, V. K. Yachandra, P. Wernet, and J. Yano, "Resonant X-ray emission spectroscopy from broadband stochastic pulses at an X-ray free electron laser", *Commun. Chem.* **4**, 84 (2021).

[7] C. Svetina, A. Abrami, I. Cudin, C. Fava, S. Gerusina, R. Gobessi, L. Rumiz, G. Sostero, M. Zangrando, D. Cocco, "Characterization of the FERMI@Elettra's on-line photon energy spectrometer" *Proc. of SPIE* **8139** 81390J-1(2011).

[8] O. Y. Gorobtsov, G. Mercurio, F. Capotondi, P. Skopintsev, S. Lazarev, I. A. Zaluzhnyy, M. B. Danailov, M. Dell'Angela, M. Manfredda, E. Pedersoli, L. Giannessi, M. Kiskinova, K. C. Prince, W. Wurth, and I. A. Vartanyants, "Seeded X-ray free-electron laser generating radiation with laser statistical properties", *Nat Commun* **9**, 4498 (2018).

[9] R. J. Glauber, "The quantum theory of optical coherence", *Phys. Rev.* **130**, 2529 (1963).

[10] A. Singer, U. Lorenz, F. Sorgenfrei, N. Gerasimova, J. Gulden, O. M. Yefanov, R. P. Kurta, A. Shabalin, R. Dronyak, R. Treusch, V. Kocharyan, E. Weckert, W. Wurth, and I. A. Vartanyants, "Hanbury Brown and Twiss Interferometry at a Free-Electron Laser", *Phys. Rev. Lett.* **111**, 034802 (2013); **117**, 239903(E) (2016).

[11] C. Gutt, P. Wochner, B. Fischer, H. Conrad, M. Castro-Colin, S. Lee, F. Lehmkuhler, I. Steinke, M. Sprung, W. Roseker, D. Zhu, H. Lemke, S. Bogle, P. H. Fuoss, G. B. Stephenson, M. Cammarata, D. M. Fritz, A. Robert, and G. Grübel, "Single Shot Spatial and Temporal Coherence Properties of the SLAC Linac

Coherent Light Source in the Hard X-Ray Regime", *Phys. Rev. Lett*. **108**, 024801 (2012).
[12] O. Y. Gorobtsov, G. Mercurio, G. Brenner, U. Lorenz, N. Gerasimova, R. P. Kurta, F. Hieke, P. Skopintsev, I. Zaluzhnyy, S. Lazarev, D. Dzhigaev, M. Rose, A. Singer, W. Wurth, and I. A. Vartanyants, "Statistical properties of a free-electron laser revealed by Hanbury Brown-Twiss interferometry", *Phys. Rev. A* **95**, 023843 (2017).
[13] A. A. Lutman, Y. Ding, Y. Feng, Z. Huang, M. Messerschmidt, J. Wu, and J. Krzywinski, "Femtosecond x-ray free electron laser pulse duration measurement from spectral correlation function", *Phys. Rev. Spec. Top-Ac.* **15**, 030705 (2012).
[14] I. A. Vartanyants and R. Khubbutdinov, "Theoretical analysis of Hanbury Brown and Twiss interferometry at soft-x-ray free-electron lasers", *Phys. Rev. A* **104**, 023508 (2021).
[15] E. Saldin, E. V. Schneidmiller, and M. V. Yurkov, "The physics of free electron lasers", *Springer* p.369 (2000).
[16] P. Pääkkönen, J. Turunen, P. Vahimaa, A. T. Friberg, and F. Wyrowski, "Partially coherent Gaussian pulses"*, Opt. Commun.* **204**, 53 (2002).
[17] H. Lajunen, J. Tervo, and P. Vahimaa, "Theory of spatially and spectrally partially coherent pulses", J. *Opt. Soc. Am. A* **22**, 1536 (2005).
[18] R. Khubbutdinov, N. Gerasimova G. Mercurio, D. Assalauova, J. Carnis, L. Gelisio, L. Le Guyader, A. Ignatenko, Y. Y. Kim, B. E. Van Kuiken, R. P. Kurta, D. Lapkin, M. Teichmann, A. Yaroslavtsev, O. Gorobtsov, A. P. Menushenkov, M. Scholz, A. Scherz, and I. A. Vartanyants, "High spatial coherence and short pulse duration revealed by the Hanbury Brown and Twiss interferometry at the European XFEL", *Structural Dynamics* **8**, 044305 (2021).